Origin of the very metal poor stars in the disk of the Milky Way

Author: Albert Ventura Nasarre
Facultat de Física, Universitat de Barcelona, Diagonal 645, 08028 Barcelona, Spain.

Advisor: Maria Teresa Antoja Castelltort

Abstract: The stars with quasi-primordial chemistry are remnants of the early stages of formation of our Galaxy thus providing insights into its assembly. We use GARROTXA, a "Milky Way-like" high resolution zoom-in cosmological simulation, to show that even though these stars are commonly associated with the halo of the Galaxy, by setting geometrical and dynamical constraints we managed to detect 619 ultra metal-poor stars with planar orbits that show a slight preference for prograde motion (around $\sim 7\%$ above the expected value of 0.5). The fraction of ultra metal-poor prograde orbits that we find is smaller than in other simulations of previous studies and than the observed fraction in the Milky Way. Moreover, we traced those stars back to our earliest available snapshot ($t = 1.87$ Gy after the Big Bang) and proved that all of them (except two) belonged to the primordial blocks from which the proto-galaxy was formed. Finally, we conclude that low metallicity stars are excellent indicators about the history of formation and assembly of its galaxy.

I. INTRODUCTION

The most metal-poor stars in the Milky Way (MW) allow us to take a glimpse at the early stages of formation and assembly of our Galaxy. These stars are thought to have formed while the MW was still in a process of assembly. Therefore, these stars are expected to be either ingrained in the deepest parts of the MW potential if they were born during the early stages of galaxy formation or that they dynamycally inhabit the halo if they have been accreted from dwarf galaxies later on, as mentioned by Sestito et al. [3]. Either way, these stars are expected to be halo-like, follow an isotropic distribution and in the case that they happen to geometrically coincide with the disk, we should expect them to show no preference for prograde or retrograde orbits.

However, recent studies using the Pristine [10] and LAMOST [11] surveys have shown that 31% of the very metal-poor stars ($[Fe/H] \leq -2.5$) that currently reside in the disk do not venture outside of it [2] and that out of 42 ultra metal-poor (UMP, $[Fe/H] \leq -4$) stars, around $\sim 26\%$ are on prograde orbits confined to 3 kpc of the MW plane [1]. In another study they also find that more than 70% of the very metal-poor stars near the disk are on prograde orbits [5]. In those studies, three different scenarios about the origin of this unconventional behaviour are hypothesized [1]. The authors suggest that (a) these stars were directly formed inside the disk, (b) these stars have been brought by the accretion of a massive dwarf galaxy, and/or (c) these stars belonged to the building blocks of the proto-MW and were introduced to the disk due to some additional mechanism.

Here we investigate the dynamics of the low metallicity stars that inhabit the disk, with a special focus on UMP stars, using simulation data from GARROTXA [6]. We find that there is a significant fraction of UMP stars with prograde orbits in the disk region and trace them back to the early stages of galactic formation to better understand this behaviour that escapes conventional beliefs.

This work is organized as follows: In sect. II we introduce the simulation as well as some specifics that were taken into account during the analysis. In sect. III we describe the calculations and statistical analysis performed during this project. In sect. IV we present the results. Finally, in sect. V we compare our results to observations and other simulations and present our final conclusions.

II. SIMULATION

In order to perform this study, we analyzed data from the GARROTXA [6] set of high-resolution cosmological zoom-in simulations. GARROTXA provides us with a series of snapshots in time that reproduce the evolution of a "Milky Way-sized" galaxy, taking into consideration interstellar gas, dark matter, and stars.

These snapshots allow us to access several physical quantities such as the positions of the stars in cylindrical coordinates (R,ϕ,z), their velocities (V_R, V_ϕ, V_z), their age, their mass, as well as chemical properties such as the metallicity. It must be noted that the coordinate system of this simulated galaxy is a right-handed one in such a way that a prograde motion will correspond to a negative value of V_ϕ for the galaxy rotating clockwise.

In this work, we focus on the study of low metallicity stars as well as their dynamical properties in the galactic disk region. The metallicities provided by GARROTXA show values significantly lower than those observed. There are several possible reasons for this discrepancy. (1) GARROTXA's supernova/AGN feedback is not as efficient as it is in the real universe; (2) GARROTXA's initial values for the metallicity are different from the "initial values of the universe"; (3) Current observations of the metallicity are unable to go beyond a certain threshold value, whereas in a simulated environment this limitation does not exist. The study of these subjects is out of the scope of this work, but what we did is to perform a logarithmic shift using the following

expression $[Fe/H]_{new} = log_{10}(10^{[Fe/H]_{old}} + 10^{[Fe/H]_{min}})$ so that the values for the metallicity are capped by the lowest metallicity ever observed ($[Fe/H]_{min} = -6.2$) [7].

In order to select what we consider the disk region, we introduce a set of geometrical constraints on the z and R components ($|z| \leq 3$ kpc and $r \leq 20$ kpc). These constraints allow us to focus on a planar region in which around $\sim 91\%$ of the stars are contained, which is consistent with the knowledge we have of the MW, while also working as a first approximation to remove stars residing in the halo and the outer regions. In sect. IV we introduce a second cut on J_ϕ that help us to further bin them into different dynamical populations.

III. METHODOLOGY

A. Action computation

In order to determine whether the stars dynamically inhabit the disk, we cannot rely solely on the aforementioned geometrical constraints, since we would not be able to discard any stars from outside of the disk that are currently traversing it. To further analyse the low metallicity populations that dynamically inhabit the disk, we decided to use action variables (J_R, J_ϕ, J_z) as a new constraint. Action-angle variables correspond to the canonical transformation $(q, p) \rightarrow (\Phi, J)$ and provide a powerful and elegant method to exploit Hamiltonian mechanics by allowing us to determine the frequencies of periodic motion without having to calculate the exact trajectories.

Since simulated galaxies are not models of the MW, there might be significant differences in their kinematics due to the fact that the spatial and mass distribution of particles in the simulated environment can differ from real MW data. As mentioned in [3], one way to minimize the effects this may have on our results is to scale each action by its norm. Furthermore, normalizing each value allows us to properly compare different data points and determine their main mechanism of motion, and thus avoid dependencies with the position that would appear if we were to use, for example, directly the angular momentum (i.e., un-normalized J_ϕ).

To obtain the action vector, we used the AGAMA package [8], which allows us to numerically derive the gravitational potential from the N-body snapshots for the gas, dark matter, and stars. AGAMA requires us to specify the symmetry of our system, in this case axisymmetric, to then represent the potential as a sum of Fourier terms in the azimuthal angle (Azimuthal Harmonic Expansion). Once the potential has been obtained, the action vector can be derived via the "Stäckel fudge" approach. This approximates the obtained potential using Stäckel potentials, which are one of the few cases for which actions can be computed analytically.

B. Statistical analysis and error computation

Once the actions are computed, we can determine which orbits are prograde ($J_\phi < 0$) or retrograde ($J_\phi > 0$) and by setting a certain threshold on $\frac{J_\Phi}{J}$ we can restrict them to being planar. We classified each star into one of three categories: prograde planar, retrograde planar, and *"other"*, where we would include halo-like orbits, highly eccentric orbits, and vertically hot orbits.

In this work, we look for the metal-poor stars in the simulation that are dynamically part of the disk. In order to do so, we are mostly interested in comparing the prograde and retrograde categories. In order to quantify the imbalance between prograde and retrograde orbits, we compute the fraction $\frac{N_{pro}}{N_{pro}+N_{ret}}$ and estimate its error.

We can infer the uncertainty associated to N_{pro} by following Bayes' theorem. We consider N_{pro} to have a binomial likelihood and we set a uniform prior since there should not be any preferential direction for the rotation. In this way, the posterior distribution is defined by:

$$\mathcal{P}(p|N_{pro}, N_{tot}) \propto \mathcal{L}(N_{pro}|p, N_{tot})\mathcal{P}(p)$$

where p is the true fraction of prograde stars, N_{pro} is the observed number of prograde stars and N_{tot} is the total number of stars. In order to derive the error, the following assumptions were made: (1) We assume that ignoring the *"other"* category in such a way that $N_{tot} = N_{pro} + N_{ret}$ becomes the true total number of stars in the probability distribution, will not introduce any extra uncertainty (2) We assume that N_{tot} does not have any error; (3) We consider the observed fraction as the true fraction when deriving the posterior distribution.

IV. RESULTS

A. Action space and fraction of prograde stars

As mentioned in sect. III A, actions allow us to properly analyse dynamical populations. To be more precise, J_ϕ can give us an idea on the *"degree"* of rotation of a given star, J_r gives us an idea on the eccentricity of its orbit and, finally, J_z gives us information on how vertically *hot* that orbit is.

In FIG. 1 we show the actions of the stars in the GARROTXA simulation at redshift 0 that have been computed with AGAMA. On the top and bottom panels, we show a density plot for all stars (top) and for only the UMP stars (bottom) within our geometrical cut ($R \leq 20$ kpc and $|z| \leq 3$ kpc). On the y-axis we represent the quantity $\frac{J_z - J_R}{J}$ and on the x-axis $\frac{J_\phi}{J}$. We chose to use $\frac{J_z - J_R}{J}$ because it allows us to include both the vertical and the radial components in the figure's axes. In the middle panel we show the distribution of UMP stars in the action space. On the horizontal axis we show $\frac{J_\phi}{J}$, on the vertical axis $\frac{J_z}{J}$, and $\frac{J_R}{J}$ is represented as a color code.

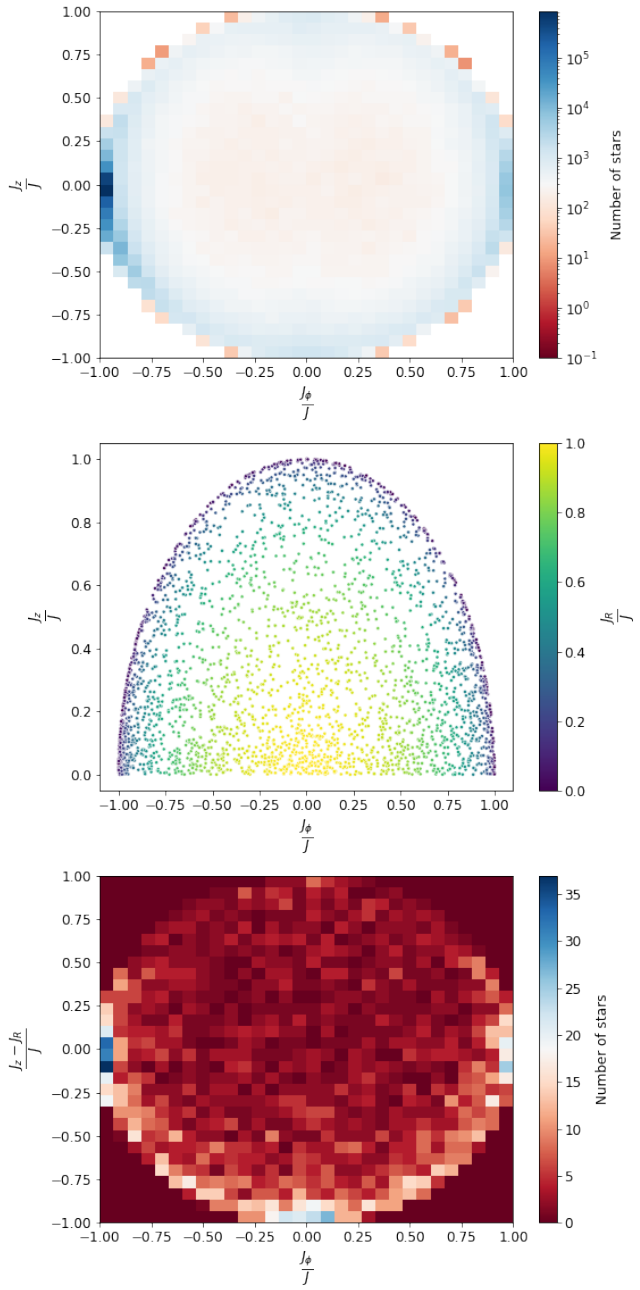

FIG. 1: *Top and bottom panels*: Density plots at redshift 0 of the distribution of all stars (top) and only the UMP stars xº(bottom) in the action space. *Middle panel*: Representation of the action space ($\frac{J_R}{J}$, $\frac{J_\phi}{J}$, $\frac{J_z}{J}$) for all UMP stars that geometrically inhabit the disk where each action is divided by its norm at redshift 0.

In the top panel, we can see that even though the entire action space is fairly populated, it is absolutely dominated by prograde rotating stars (deep blue in the leftmost part of the figure). In the middle panel we can distinguish that UMP stars show some sort of preference for planar motion, which in the figure corresponds to the regions with a high absolute value of the azimuthal action and low values of the vertical and radial actions (i.e. lower left and lower right sides of the figure with a darker color). In the bottom panel, we can clearly distinguish three regions with a density considerably higher than the rest. Firstly, we have an area with a high negative value of $\frac{J_z - J_R}{J}$ and with practically no rotation. This corresponds to highly eccentric stars (high J_R) and coincides with the yellow area on the middle panel. Although this is interesting, this region is not the subject of our study and we did not investigate it further.

Finally, we can see two other regions that correspond to high values of the absolute value of $\frac{J_\phi}{J}$. These regions are made of stars with a planar rotation and we see that there is a higher density of prograde stars with disk-like orbits ($\frac{J_\phi}{J} < 0$) than of retrograde stars ($\frac{J_\phi}{J} > 0$).

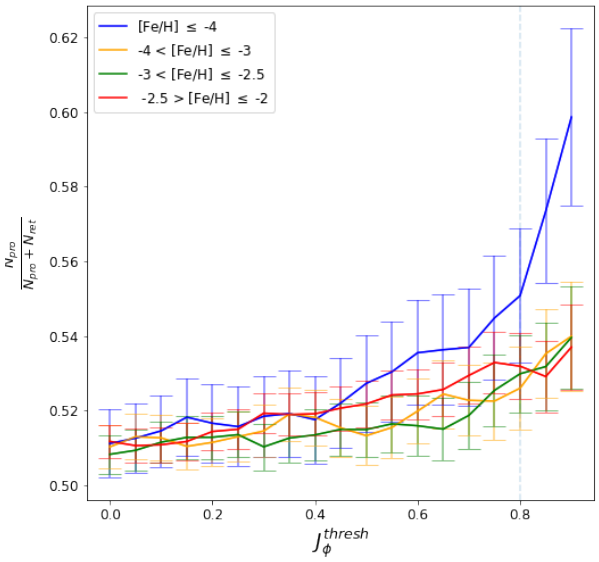

FIG. 2: Fraction $\frac{N_{pro}}{(N_{pro}+N_{ret})}$ as a function of different values for J_ϕ^{thresh} where each color represents a different metallicity bin in the low metallicity regime ($[Fe/H] \leq -2$). The dashed vertical line shows the 0.8 mark after which the fraction for UMP stars increases considerably compared to the rest. The uncertainties associated to the fraction have been computed following the procedure mentioned in sect. III B within a 68.2% confidence interval.

In order to better understand this preference for prograde orbits, we separate our stars into three different categories by setting a threshold value on the azimuthal action J_ϕ^{thresh} in such a way that $\frac{J_\phi}{J} > J_\phi^{thresh}$ corresponds to a retrograde motion and $\frac{J_\phi}{J} < -J_\phi^{thresh}$ corresponds to a prograde motion. Any other value is categorized as *"other"*. Then, we compute the fraction $\frac{N_{pro}}{N_{pro}+N_{ret}}$ for different metallicity bins and for different threshold values following the error computation mentioned in sect. III B. Previously, we mentioned that low metallicity stars are expected to be found with halo-like

isotropic distributions. Nevertheless, in FIG. 2 we can clearly see that there is a slight preference for prograde orbits in all low metallicity curves and that this preference becomes more significant the higher the value of J_ϕ^{thresh} is. Albeit all curves are comparable within the error range along almost all threshold values, the prograde fraction for the UMP stars remains higher compared to the other metallicity curves showing an extremely substantial increase for $J_\phi^{thresh} > 0.8$ (marked with a blue dashed vertical line).

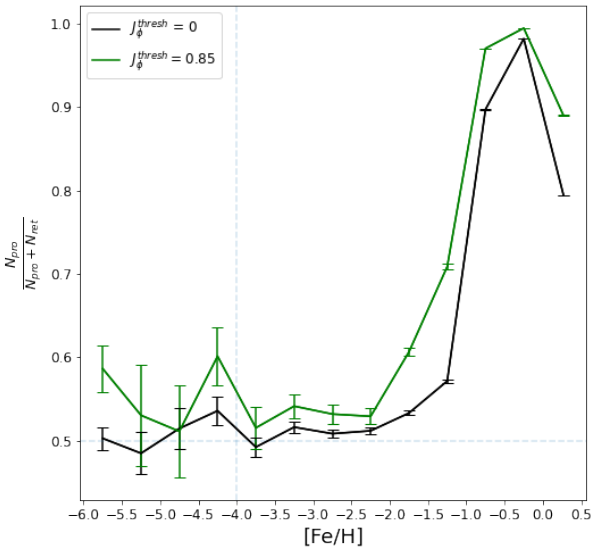

FIG. 3: Fraction $\frac{N_{pro}}{N_{pro}+N_{ret}}$ as a function of the metallicity at redshift 0. The results are shown for $J_\phi^{thresh} = 0$ and $J_\phi^{thresh} = 0.85$ in black and green, respectively. The vertical and horizontal dashed lines work as a visual support. They show the limit in which the UMP regime ends and the threshold for which $N_{pro} = N_{ret}$, respectively.

Given the substantial increase for prograde UMP stars shown in FIG. 2, we set our threshold value for the azimuthal action at $|\frac{J_\phi}{J}| = 0.85$. The exact number of prograde and retrograde stars and the fraction for this threshold are given in the second column of TABLE I.

In FIG. 3 we plot the fraction of prograde orbits as a function of the metallicity in order to better understand the behaviour of the disk region in this regard. We separate the plot into two curves to compare the effects of using the aforementioned threshold in the azimuthal action as opposed to using a naive separation at $\frac{J_\phi}{J} = 0$. It can clearly be seen that when we use the naive approach the fraction of prograde orbits remains around 0.5 for UMP stars due to the fact that this region is being dominated by halo stars with no rotation. In contrast, when we use the azimuthal action constraint, the prograde fraction shows points where there are up to $\sim 10\%$ more prograde orbits than the expected value of 0.5.

As we increase in metallicity, in the region $-4 < [Fe/H] < -2$, we can still see a slight preference for prograde orbits when the dynamical cut is in place as opposed to the dominance of halo stars for $J_\phi^{thresh} = 0$ (fraction closer to 0.5).

In the region $-2 < [Fe/H] < -1$ we begin to see a gradual increase in the fraction of prograde rotating stars as the metallicity gets higher. This is likely associated with stars from the thick disk.

Finally, we can see a region where the fraction of prograde orbits reaches a value of ~ 1. These are young, metallic stars that have been born within the disk and have been chemically enriched by successive star formation and evolution associated with this region. The most metallic stars ($[Fe/H] > 0$) show a sudden drop in prograde orbits. We studied the distribution of stars in this region and discovered that these stars are very young and reside at very low radii ($\sim$ 0.6 kpc) where orbits can become hotter (i.e., the known increasing velocity dispersion towards the inner regions of disk galaxies).

B. Tracing the UMP stars

In sect. IV A, we found that there are some UMP stars that currently inhabit the disk and have planar orbits. To understand their origin, we cross-matched the particles IDs between the snapshot corresponding to the present (t = 13.86 Gy) and one of the earliest that we have available for this simulation (t = 1.87 Gy) which happens to be several Gy before a major merger event that took place in this galaxy (around $t = 4.71$ Gy).

In FIG. 4 we show the projection on the X-Y plane at t = 1.87 Gy of all the stars that are geometrically inside the disk in the present (gray), and all UMP stars with prograde and retrograde orbits (blue and red respectively). We can clearly distinguish two main galaxies and have drawn a dashed line so that the two systems can be set apart. On the bottom left there is what we dubbed as Galaxy 1 (G.1) and on the top right Galaxy 2 (G.2).

We analysed the number of stars that belong to each system and present the results in TABLE I, where we see that all UMP stars (except two of them that were in distant, smaller systems and were not taken into account) that we consider planar (i.e., those that have $|\frac{J_\phi}{J}| \geq 0.85$ at redshift 0) were already present in G.1 and G.2. Moreover, we find that out of all the stars that end up with prograde planar orbits, around $\sim 60\%$ come from G.2.

V. CONCLUSIONS

Using GARROTXA's cosmological zoom-in simulation and analysing the action space at redshift 0, we managed to find that there is a slight preference for prograde orbits for low metallicity stars that are confined to the galactic plane. This preference for prograde orbits is higher for UMP stars and becomes increasingly significant the

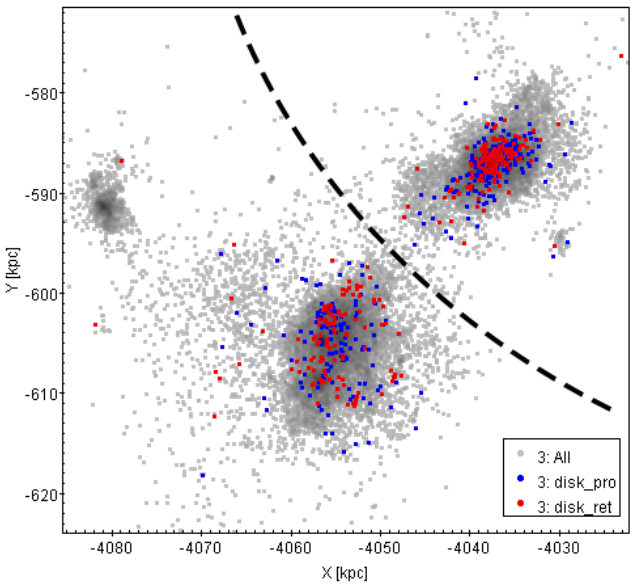

FIG. 4: Projection on the X-Y plane at $t = 1.87$ Gy of all the stars that are geometrically inside the disk at $t = 13.86$ Gy (gray), and all UMP stars with planar prograde and retrograde orbits (blue and red respectively). The dashed line separates the two systems, which we refer to as G.1 (bottom left) and G.2 (top right).

	$t = 13.86$ Gy	G.1 ($t = 1.87$ Gy)	G.2 ($t = 1.87$ Gy)
N_{pro}	355 ± 12	138 ± 8	217 ± 9
$N_{pro} + N_{ret}$	619	258	359
$\frac{N_{pro}}{N_{pro}+N_{ret}}$	0.57 ± 0.02	0.53 ± 0.03	0.60 ± 0.03

TABLE I: The number of stars with prograde orbits N_{pro}, the total number of stars with planar orbits $N_{pro} + N_{ret}$, and the ratio $\frac{N_{pro}}{N_{pro}+N_{ret}}$ using $J_\phi^{thresh} = 0.85$, are reported for the disk at $t = 13.86$ Gy and traced back to $t = 1.87$ Gy for the two systems G.1 and G.2 shown in FIG. 4.

higher the threshold value on the azimuthal action is, reaching up to $\sim 7\%$ for $J_\phi^{thresh} = 0.85$. In [3] the authors used 5 high-resolution cosmological zoom-in simulations from the NIHAO-UHD project and obtained values $\frac{N_{pro}}{N_{ret}} \geq 2$ for all of them. Interestingly, the preference that we find for prograde orbits is significantly smaller compared to their simulations. This likely means that those galaxies have had a significantly different assembly story compared to GARROTXA's one.

They also perform their analysis on the few known UMP stars from the MW which yields $\frac{N_{pro}}{N_{ret}} = 11$. It must be noted that only 42 UMP stars are known for the MW for which the fraction can be a subject of poor statistics. Hopefully, the release of Gaia DR3 (Gaia Collaboration, Vallenari, et al., 2022, in prep.) and other dedicated spectroscopic surveys will provide us with more data and allow us to obtain more accurate results.

After tracing the UMP stars back to $t = 1.87$ Gy, we prove that all of them belong to the primordial blocks of the simulated galaxy, discarding the hypotheses that they were directly created inside the disk or that they were accreted from dwarf galaxies. Furthermore, we discovered that around $\sim 60\%$ of the stars with disk-like orbits ($\frac{J_\phi}{J} \leq -0.85$) at redshift 0 come from G.2, which hints to us that something happened during the merger that brought those stars into the disk.

There are several possibilities which may have caused these UMP stars to adopt planar orbits. It could be associated directly with the merger of these primordial blocks or could have been caused by later events which may have "flattened" the ancient halo. To better understand the exact origin of these disk-like UMP stars we would need to preform further analyses throughout all times, which is out of the scope of this work.

All of these results show clear evidence that the dynamics of low metallicity stars open a window to the past that provides us insight into the galaxy's early stages of formation.

Acknowledgments

I want to express my gratitude to my advisor Teresa Antoja for all her guidance and the knowledge she has imparted to me. I am also immensely grateful to Santi Roca-Fàbrega and Begoña García-Conde from Universidad Complutense de Madrid for their willingness to help during the project. Finally, I would like to thank my family and friends for all their love and support.

[1] Sestito, F., Longeard, N., Martin, N. F., et al. (2019). MNRAS, 484(2), 2166-2180.
[2] Sestito, F., Martin, N. F., Starkenburg, E., et al. (2020). MNRAS: Letters, 497(1), L7-L12.
[3] Sestito, F., Buck, T., Starkenburg, E., et al. (2021). MNRAS, 500(3), 3750-3762.
[4] Conroy, C., Bonaca, A., Cargile, P., et al. (2019). ApJ, 883(1), 107.
[5] Carter, C., Conroy, C., Zaritsky, D., et al. (2021). ApJ, 908(2), 208.
[6] Roca-Fàbrega, S., Valenzuela, O., Colín, P., et al. (2016). ApJ, 824(2), 94
[7] Nordlander, T., Bessell, M. S., Da Costa, et al. (2019). MNRAS: Letters, 488(1), L109-L113.
[8] Vasiliev, E. (2019). MNRAS, 482(2), 1525-1544.
[9] Buck, T., Obreja, A., Macciò, A. V., Minchev, et al. (2020). MNRAS, 491(3), 3461-3478.
[10] Starkenburg, E., Martin, N., Youakim, K., et al. (2017). The Pristine survey–I. MNRAS, 471(3), 2587-2604.
[11] Zhao, G., Zhao, Y. H., Chu, Y. Q., et al. (2012). Research in Astronomy and Astrophysics, 12(7), 723.